

Modeling of IGBT junction temperature based on load torque variation in induction motor

Ahmed Shihab Mayyahi, Riyadh Ghanem Omar

Department of Electrical Engineering, College of Engineering, Mustansiriyah University, Baghdad, Iraq

Article Info

Article history:

Received Sep 22, 2022

Revised Dec 31, 2022

Accepted Jan 15, 2023

Keywords:

Air force cooling

Inverter losses

SIMSCAPE

Space vector PWM

Thermal resistance

ABSTRACT

In order to discuss the effectiveness of inverter performance, it is essential to concentrate on its losses. Thus, knowing the junction temperature (TJ) value of the inverter switches insulated-gate bipolar transistor (IGBTs) under different loading conditions allows determining their reliability and designing the right heat sink. The old methods to calculate the TJ are inaccurate, difficult to implement, and require mathematical analysis. So, in this work, a new approach was used to calculate the TJ in a simplified way, using the SIMSCAPE environment in the MATLAB simulation. The IGBT in the SIMSCAPE environment is of an improved design and has a direct thermal port. The TJ estimation is more accurate and it relies only on the thermal impedance model, so we do not need to compute the power losses as was done in previous studies. This functionality is only accessible in more recent versions of MATLAB (2019-2023). With different motor load torques, the IGBT junction temperature is evaluated, and the effect of the selected heat sink on the value of TJ is evaluated when it is under the effect of natural cooling and air-forced cooling.

This is an open access article under the [CC BY-SA](https://creativecommons.org/licenses/by-sa/4.0/) license.



Corresponding Author:

Ahmed Shihab Mayyahi

Department of Electrical Engineering, College of Engineering, Mustansiriyah University

Baghdad, Iraq

Email: eema2002@uomustansiriyah.edu.iq

1. INTRODUCTION

Power electronics (PE) devices are widely used in industrial and household settings in contemporary civilization for purposes of controlling and producing electricity [1]. Power transistors, particularly insulated-gate bipolar transistor (IGBT) modules, are in control of the power converter industry thanks to their superior performance, inexpensive cost, dependability, lightweight, wind power generation, and motor drives [2]. The semiconductor devices' operating junction temperature has a significant influence on IGBT power modules' lifespan [3]. One of the most important factors to take into account is the junction temperature, which is directly related to inverter power loss and overheating. These elements can lead to wear and tear as well as failures. The semiconductor chip junction temperature prediction is necessary to achieve accurate measurement and avoid chip burning [4]. Many approaches to simulating the junction temperature were previously in place, such as finite element simulation and three-dimensional modeling, while the two approaches above make it impossible to extract the internal and structural parameters [5], [6]. In addition to the most common method, which is to make a two-part simulation through coupling, the RC network model and loss calculation model, which are built on the foundation of a data sheet, are then electro-thermally coupled, with the relevant parameters of the inverter system being entered into the loss calculation model to obtain the thermoelectric simulation [7]. In this study, the junction temperatures of all IGBTs can be directly estimated by using the SIMSCAPE environment in MATLAB/Simulink and building an impedance thermal

model alone based on the manufacturer's data. This work focused on overcoming these restrictions and developing a junction temperature estimating system that included various load patterns for induction motors and types of applied coolant systems.

2. METHOD

2.1. Thermal resistance model

As inverters have been developed to drive induction motors and supply important applications, it has become crucial to understand how to regulate the IGBT junction temperature, which is the power module of an inverter. The IGBTs are often restricted by their junction temperature, and if the junction temperature is not correctly controlled, there is a significant risk of failure due to overheating [8]. The IGBTs are responsible for all power loss; the heat produced by the IGBT is mostly transferred to the substrate, heat sink, and air through heat conduction. As a result, the thermal resistance of the IGBT module's entire heat transfer process can be divided into only three components. The IGBT chip's thermal resistance to the heat sink is initially measured as its contact thermal resistance, followed by the heat sink's solid thermal resistance and the heat sink's convective heat transfer resistance to the ambient [9], [10].

Actually, the heat dissipation route diagram's shows that the thermal resistance between the chip and the heatsink is the total thermal resistance of each layer in series [11], as illustrated in (1).

$$RJA = RJC + RCH + RHA \quad (1)$$

The following equation represents each layer's thermal resistance and heat capacity:

$$R_{th} = \frac{L}{kA} \quad (2)$$

$$C_{th} = cpAL \quad (3)$$

where, R_{th} is the thermal resistance per each layer, L is its thickness, k is its thermal conductivity, A is its area for dissipating heat, C_{th} is the material's total heat capacity, c is its specific heat capacity, and r is its density. For an accurate TJ estimate and a consistent conformance of its junction temperature, the IGBT module in the three-phase inverter employs the junction temperature estimation approach. This task can be achieved by simulating the thermal network model (Foster model) using MATLAB/Simulink SIMSCAPE environment, which were created with the manufacturers document in [12]. Figure 1 represent the IGBT and the freewheeling diode module's complete heat transfer process in the thermal resistor network [13].

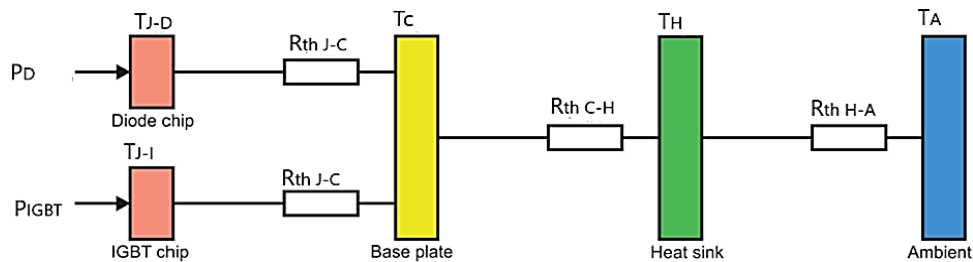


Figure 1. Heat transfer mechanism

2.2. Heat sink characteristics

To keep the device junction temperature at a low-level during power flow through it, it is important to select a heat sink in accordance with chip losses [14]. Conduction and convection-type heat transfer are used by the majority of electronic device cooling systems for thermal management [15]. The heat sink material and size are taken into consideration when the amount of power dissipation in the device rises, and the material's thermal conductivity should be as high as feasible. The finned extruded aluminum form is the most often utilized kind of heat sink that is commercially available, as shown in Figure 2.

This fundamental radiator form is best for forced air and natural convection cooling because a large surface area is exposed to the surrounding air inside a small area. The capacity of aluminum to transfer heat to the ambient is measured in °C/W of power dissipation to choose the appropriate kind of heat sink, consider

the power dissipation and thermal data from the datasheet provided by the device manufacturer, to select the heat sink, the following parameters are required: target junction temperature (T_j), maximum ambient temperature (T_a), thermal resistance value $R_{th}(ja)$, and heat sink thermal resistance value $R_{th}(sa)$ [16]. Power chips like IGBT often employ forced air cooling with a heat sink and fans to dissipate heat or liquid cooling techniques because natural convection can no longer dissipate heat due to the fast growth of IGBT modules [17]. Figure 3 demonstrates the change in the thermal resistance value of the forced-air heat sink [18]. The value of $R_{th}(ja)$ and value of $R_{th}(sa)$ can be obtained from (4) and (5).

$$R_{th}(ja) = (T_j - T_a) / P_{diss} \quad (4)$$

$$R_{th}(sa) = R_{th}(ja) - R_{th}(jc) - R_{th}(cs) \quad (5)$$

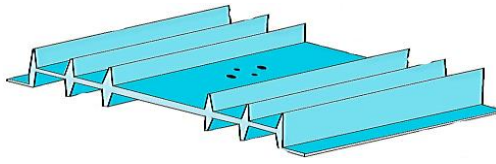


Figure 2. The common finned heat sink

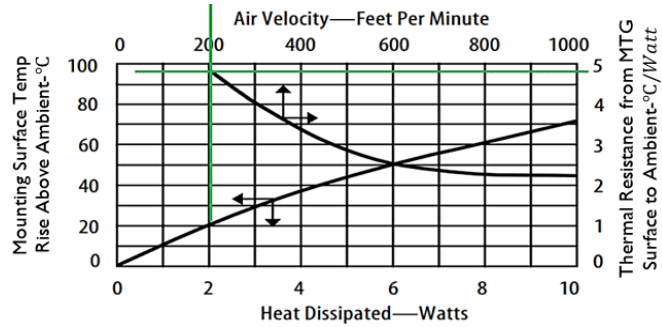


Figure 3. Heat dissipation of an IGBT

2.3. Three-phase voltage source inverter fed induction motor

Three-phase induction motors (IM) are often the most used in the industry since need less maintenance and operate with great reliability [19]. Moreover, customers are increasingly interested in highly efficient electric motors since the price of electric energy has increased in recent years [20]. Figure 4 shows a capacitor-DC link for a typical three-phase voltage-source inverter (VSI) with a six-switch connected to the three-phase IM. The three-phase voltage source inverter consists of six semiconductor switches (S_1 to S_6) that conduct in a 180° phase shift between their upper and lower switches [21]. Six operational periods are separated by 60 degrees in VSI. For the inverter to operate symmetrically, one upper switch, two lower switches, or two upper switches and one lower switch are tuned on for each interval. There are a total of eight different combinations in which the three-phase VSI may operate. These are shown by the switching positions on the top or lower side [22].

From the dynamic representation of the IM model, the three-phase currents can be presented in a three-axis coordinate. The stator current and the angular frequency, which are described in the three-phase coordinate frame as follows [23]:

$$i_{sa} = I_m \sin(\omega_o * t) \quad (6)$$

$$i_{sb} = I_m \sin\left(\omega_o * t + \frac{2\pi}{3}\right) \quad (7)$$

$$i_{sc} = I_m \sin\left(\omega_o * t + \frac{4\pi}{3}\right) \quad (8)$$

transforming the stator current from three-phase coordinate to two-phase coordinate as in [23]:

$$i_s = \frac{2}{3} (i_a + a * i_b + a^2 * i_c) \quad (9)$$

$$a = e^{j\frac{2\pi}{3}} = \left(\frac{-1}{2} + j\frac{\sqrt{3}}{2}\right) \quad (10)$$

$$a^2 = e^{j\frac{4\pi}{3}} = \left(\frac{-1}{2} - j\frac{\sqrt{3}}{2}\right) \quad (11)$$

in addition, to transform the other variables, such as electromagnetic torque (T_e), the same transformation of coordinates is used [24]:

$$V_s = R_s * i_s + \frac{d\Psi_s}{dt} + j\omega_s * \Psi_s \quad (12)$$

$$0 = R_s * i_r + \frac{d\Psi_r}{dt} + j(\omega_s - \omega) * \Psi_r \quad (13)$$

$$\Psi_s = L_s * i_s + L_m * i_r \quad (14)$$

$$\Psi_r = L_r * i_r + L_m * i_s \quad (15)$$

$$T_e = \frac{3}{2} * p * \text{Re}\{\overline{\Psi_s} * i_s\} = \frac{-3}{2} * p * \text{Re}\{\overline{\Psi_r} * i_r\} \quad (16)$$

2.4. Space vector PWM technique

Numerous industrial applications, including energy savers, motor soft starters, are utilizing different voltage modulation methods. Inverters controlled by support vector machine (SVM) provide the lowest harmonics and highest efficiency when compared to other modulation techniques [25]. Improvements in the quality and consistency of the drive circuit are becoming more and more necessary as a result of ongoing research on improving the performance of motor drives. The development of power semiconductor devices has greatly increased the power handling capacity of IGBT switches. SVM inverters are utilized extremely efficiently and affordably in low, medium, and certain high-power applications [26]. The SVPWM and its switching operation is presented in Figure 5 [27].

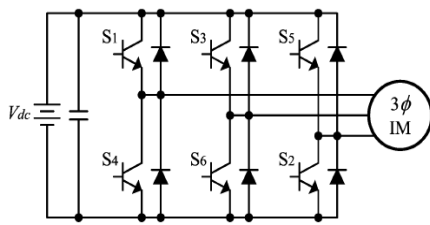


Figure 4. Three phase inverter fed IM

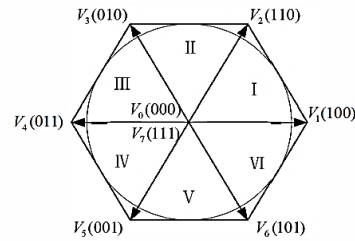


Figure 5. Space vector PWM diagram and switching operation

SVPWM samples the reference vector V^* at a frequency f_s ($T_s=1/f_s$). The alpha-beta transformation is used to create the reference vector V^* from three-phase 120° phase shift references.

$$V_\alpha = V_{an} - \frac{1}{2}V_{bn} - \frac{1}{2}V_{cn} \quad (17)$$

$$V_\beta = V_{an} - \frac{\sqrt{3}}{2}V_{bn} - \frac{\sqrt{3}}{2}V_{cn} \quad (18)$$

The magnitude of the reference voltage is given by (19).

$$V_{ref} = \sqrt{(V_\alpha)^2 + (V_\beta)^2} \quad (19)$$

There are six distinct sectors spaced 60 degrees apart on the $\alpha\beta$ -plane, the unitary ramp is generated using the ramp generator at the PWM switching frequency, the switching sequence uses this ramp as its time basis, when determining when to apply a voltage vector to a motor, the switching time calculator is employed, the block input is the sector in which the voltage vector lies, the switching time calculator and the ramp generator provide the gate logic with the timing sequence and ramp, respectively, in order to properly activate the inverter switches, this block compares the ramp and gate timing signals [28].

3. RESULTS AND DISCUSSION

The MATLAB/Simulink 2022 package is used with the SIMSCAPE environment to run the simulation. three-phase inverter with an induction motor load (IM). Figures 6 and 7 show the components of the circuit model used to simulate the proposed method. The system parameters of the simulation model were listed as follows: rated power is 7 KW, rated speed is 1800 rpm, and $p=4$. The switching frequency is 5 kHz, the fundamental frequency is 60 Hz, the DC-link voltage is 400 volts, the ambient temperature is 25 °C, and the IGBT's maximum temperature is 150 °C. The cooling system's fan speed is 1000 ft/min.

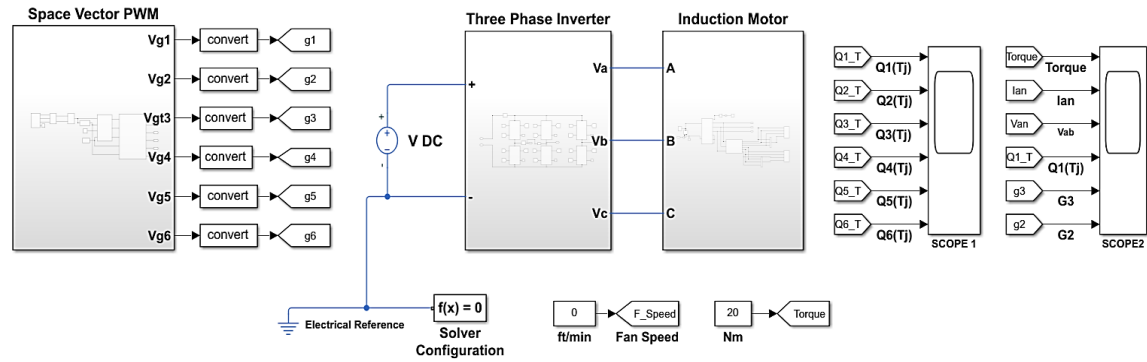


Figure 6. Block diagram of the overall system

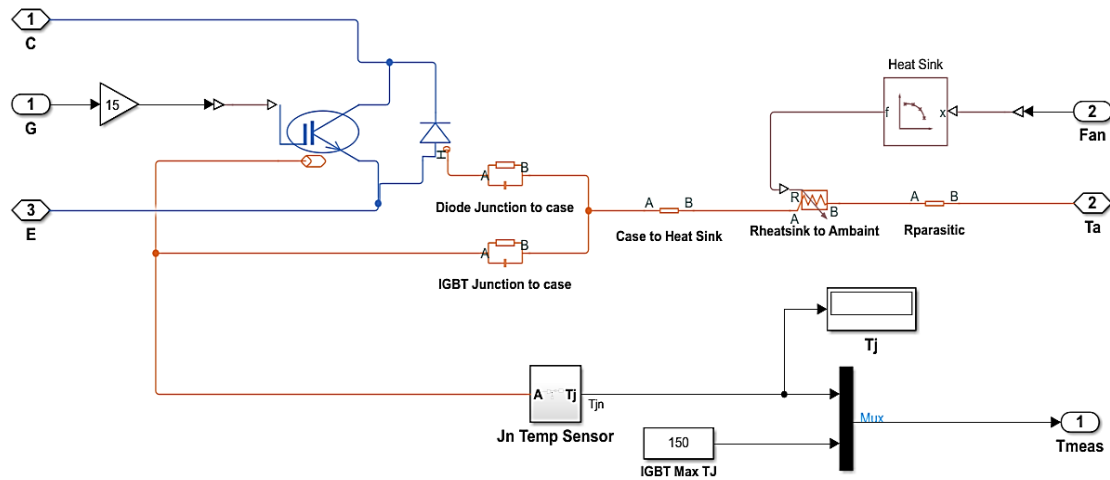


Figure 7. Thermal model of an IGBT with heat sink in SIMSCAPE environment

In this study, four load torque values (10, 15, 20, 25) Nm are used of this system to monitor changes in the junction temperature. It is found that the value of the junction temperature increases as the load torque rises; the maximum value of T_J was recorded at a torque of 10 Nm is (64.5 °C), it recorded (71.7 °C) at a torque of 15 Nm, it recorded (77.24 °C) at a torque of 20 Nm and recorded (82.46 °C) at a torque of 25 Nm. The maximum allowable T_J provided by the manufacturer is 150 °C. As illustrated in Figures 8 to 11. Figure 12 shows how the value of the junction temperature changes under the natural cooling of the heat sink when an additional load torque is applied suddenly, where the value of T_J is 83 °C. Figure 13 shows how the value of the junction temperature changes under forced air cooling of the heat sink when an additional load torque is suddenly applied, where the value of T_J recorded is 61.2 °C. Figure 14 shows the phase current and line to line voltage at load torque of 15 Nm.

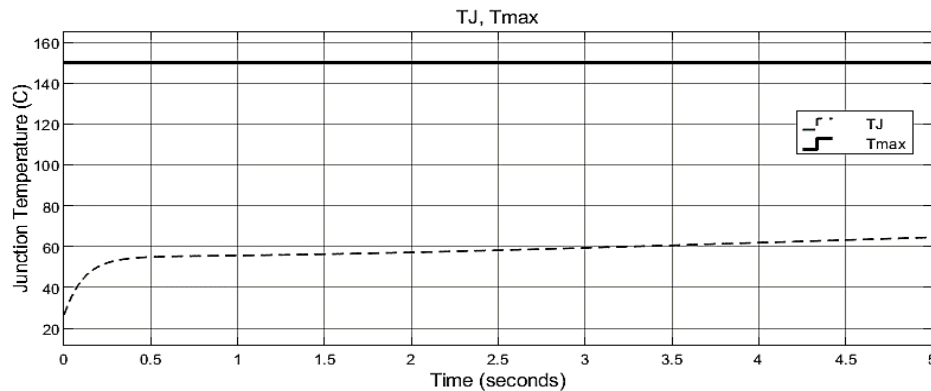


Figure 8. Junction temperature at 10 Nm

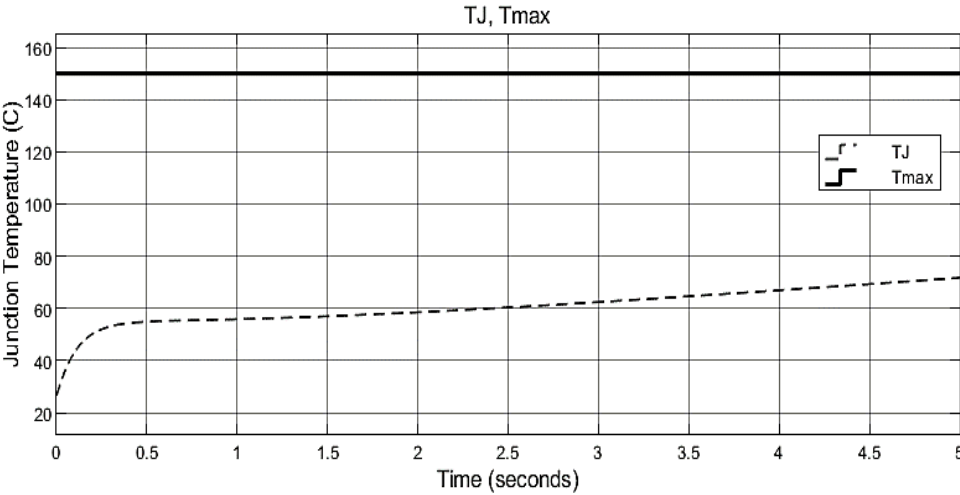


Figure 9. Junction temperature at 15 Nm

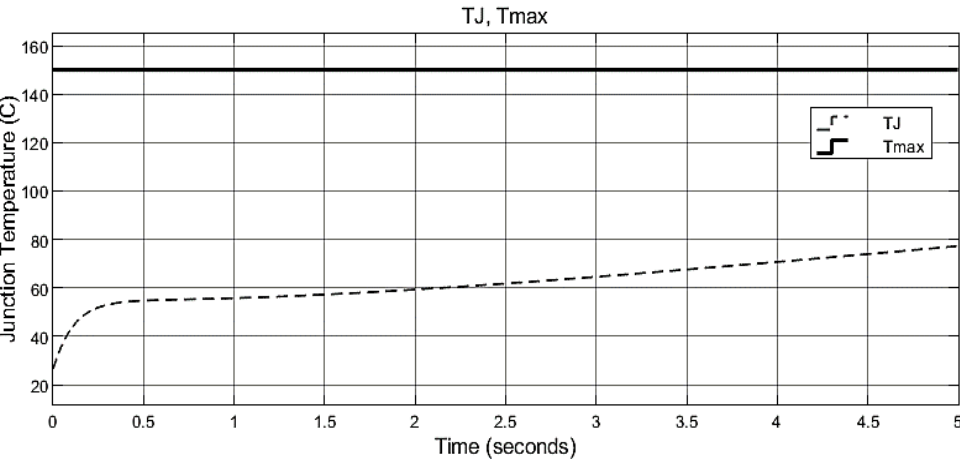


Figure 10. Junction temperature at 20 Nm

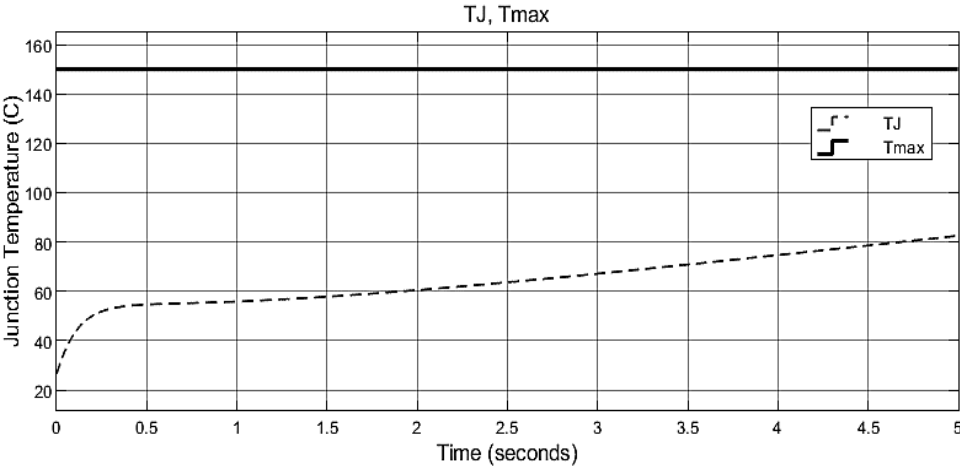


Figure 11. Junction temperature at 25 Nm

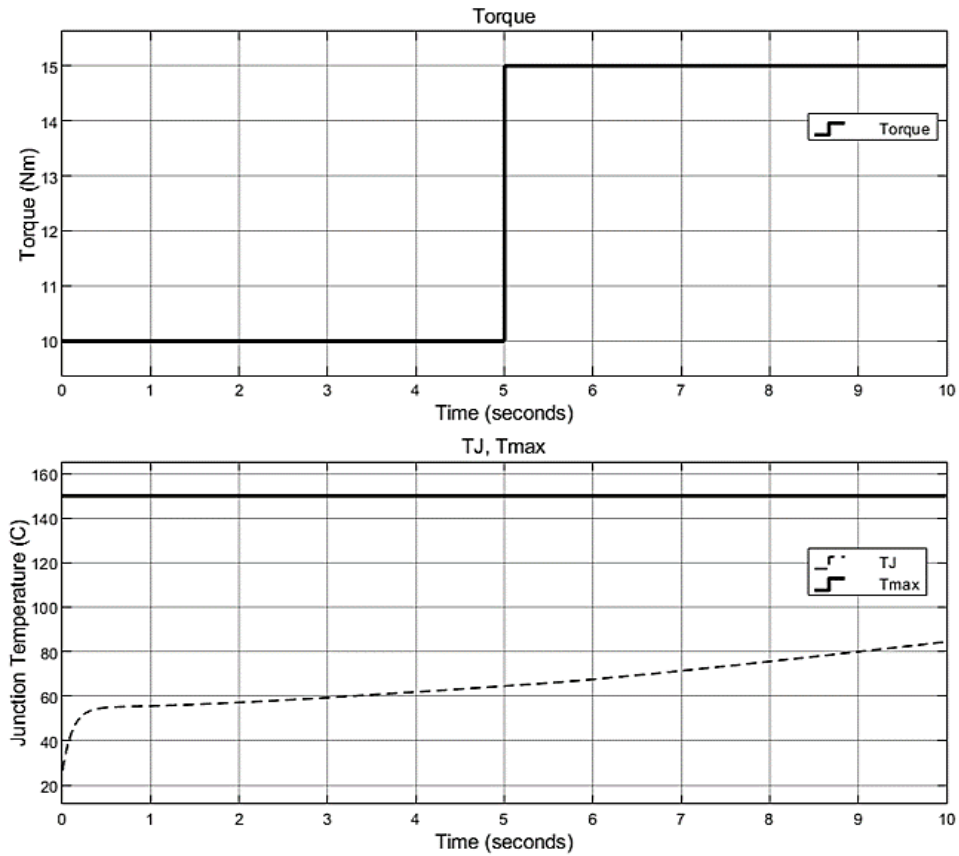


Figure 12. Junction temperature under natural cooling

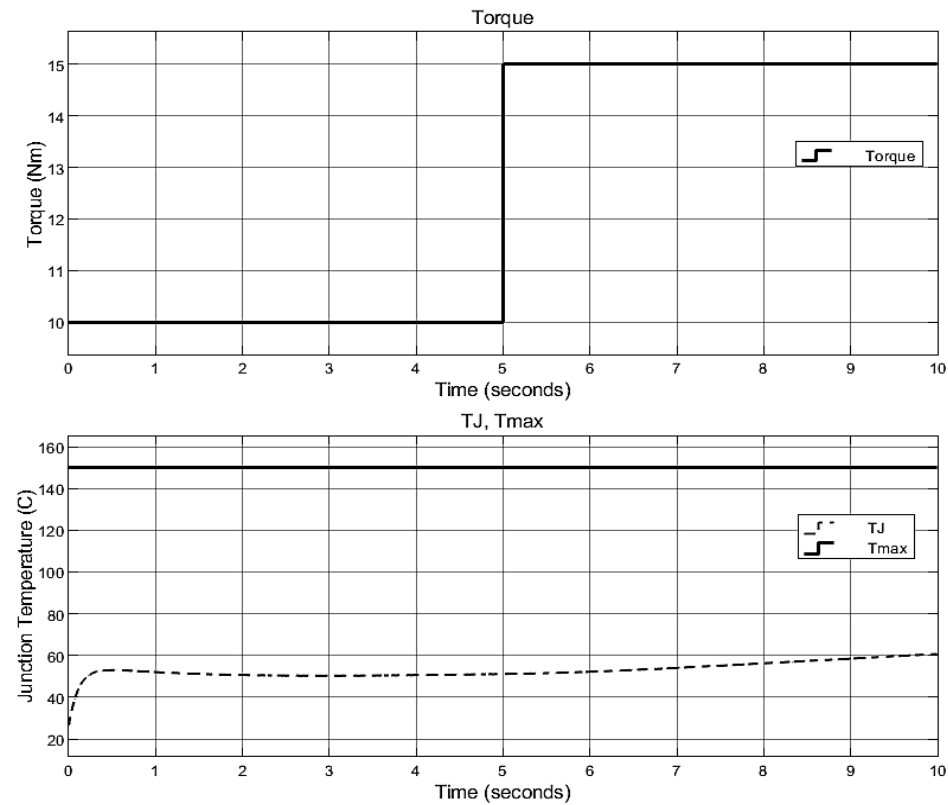


Figure 13. Junction temperature under air forced cooling

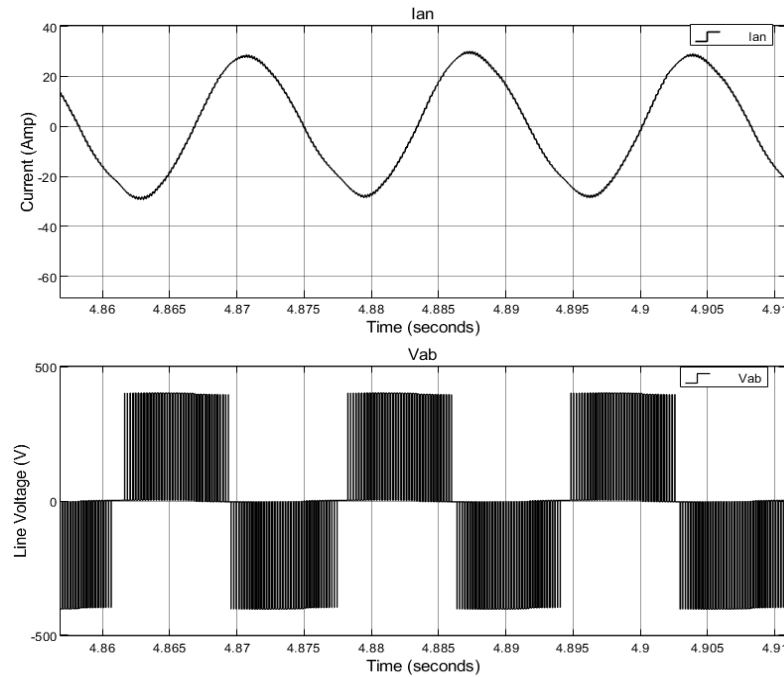


Figure 14. Line voltage V_{ab} and phase current I_{an}

4. CONCLUSION

Calculating the junction temperature for IGBT is very important because it gives a predictive indication of the power converter's efficiency. In this work, the SIMSCAPE environment was used in the MATLAB/Simulink simulation to calculate IGBT junction temperature. as a new proposed physical modeling approach. Based on this new and direct modeling, it is possible to easily obtain the value of T_J by analyzing the equivalent heat-transfer model of the IGBT module. This can be achieved only based on the manufacturer's thermal impedance information. Analytical results point to the influence of the load torque on the value of the junction temperature. The results show that the T_J increased with the increase in IM load torque. In addition, the results show that under the same working conditions of the system, but by using forced air cooling of the IGBT instead of natural cooling, the value of the junction temperature is reduced by 22 °C, and as a result. The performance of the IGBT will improve and its efficiency will increase while remaining within the allowable temperature limit.

ACKNOWLEDGEMENTS

The authors would like to thank the people who work in the Electrical Engineering Department at Mustansiriyah University for their help and advice.




REFERENCES

- [1] S. Chakraborty, B. Kramer, and B. Krepski, "A review of power electronics interfaces for distributed energy systems towards achieving low-cost modular design," *Renewable and Sustainable Energy Reviews*, vol. 13, no. 9, pp. 2323-2335, 2009, doi: 10.1016/j.rser.2009.05.005.
- [2] L. Tan, P. Liu, C. She, P. Xu, L. Yan, and H. Quan, "Heat dissipation characteristics of IGBT module based on flow-solid coupling," *Micromachines*, vol. 13, no. 4, p. 554, 2022, doi: 10.3390/mi13040554.
- [3] J. Wolfle, M. Nietzsche, J. Richardt, and J. Roth-Stielow, "Junction temperature control system to increase the lifetime of IGBT-Power-modules in synchronous motor drives without affecting torque and speed," in *IEEE Open Journal of Power Electronics*, vol. 1, pp. 273-283, 2020, doi: 10.1109/OJPEL.2020.3014443.
- [4] L. Wei, J. McGuire, and R. A. Lukaszewski, "Analysis of PWM frequency control to improve the lifetime of PWM inverter," in *IEEE Transactions on Industry Applications*, vol. 47, no. 2, pp. 922-929, 2011, doi: 10.1109/TIA.2010.2103391.
- [5] A. S. Bahman, K. Ma, and F. Blaabjerg, "A novel 3D thermal impedance model for high power modules considering multi-layer thermal coupling and different heating/cooling conditions," *2015 IEEE Applied Power Electronics Conference and Exposition (APEC)*, 2015, pp. 1209-1215, doi: 10.1109/APEC.2015.7104501.
- [6] W. Zhihong, S. Xiezu, and Z. Yuan, "IGBT junction and coolant temperature estimation by thermal model," *Microelectronics Reliability*, vol. 87, pp. 168-182, 2018, doi: 10.1016/j.microrel.2018.06.018.
- [7] X. Xin and C. Zhang, "Junction temperature estimation model of insulated gate bipolar transistor power module in three-phase inverter," *IECON 2017 - 43rd Annual Conference of the IEEE Industrial Electronics Society*, 2017, pp. 1267-1272, doi: 10.1109/IECON.2017.8216216.




- [8] H. Lim, J. Hwang, S. Kwon, H. Baek, J. Uhm, and G. Lee, "A study on real time IGBT junction temperature estimation using the NTC and calculation of power losses in the automotive inverter system," *Sensors*, vol. 21, no. 7, p. 2454, 2021, doi: 10.3390/s21072454.
- [9] X. Lin, *et al.*, "Design and analysis of the IGBT heat dissipation structure based on computational continuum mechanics," *Entropy*, vol. 22, no. 8, p. 816, 2020, doi: 10.3390/e22080816.
- [10] J. H. Lee, Y. W. Son, and S. Chang, "Numerical analysis on natural convection heat transfer in a single circular fin-tube heat exchanger (part 2): correlations for limiting cases," *Entropy*, vol. 22, no. 3, p. 358, 2020, doi: 10.3390/e22030358.
- [11] P. Górecki, K. Górecki, R. Keisel, and M. Myśliwiec, "Thermal parameters of monocrystalline GaN Schottky diodes," in *IEEE Transactions on Electron Devices*, vol. 66, no. 5, pp. 2132-2138, May 2019, doi: 10.1109/TED.2019.2907066.
- [12] Y. Yang and P. Zhang, "A novel bond wire fault detection method for IGBT modules based on turn-on gate voltage overshoot," in *IEEE Transactions on Power Electronics*, vol. 36, no. 7, pp. 7501-7512, Jul. 2021, doi: 10.1109/TPEL.2020.3047135.
- [13] R. Küenzi, "Thermal design of power electronic circuits," 2016, *arXiv: 1607.01578*.
- [14] L. Hongyi, X. Guo, and G. Chen, "Comprehensive thermal resistance model of forced air-cooling system for multiple power chips," *Energy Reports*, vol. 7, pp. 261-267, 2021, doi: 10.1016/j.egy.2021.01.071.
- [15] M. E. Kadum, A. A. Imran, and S. Aljabair, "Heat transfer in electronic systems printed circuit board: a review," *Engineering and Technology Journal*, vol. 40, no. 1, pp. 99-108, 2022, doi: 10.30684/etj.v40i1.2113.
- [16] T. Wu, Z. Wang, B. Ozpineci, M. Chinthavali, and S. Campbell, "Automated heatsink optimization for air-cooled power semiconductor modules," in *IEEE Transactions on Power Electronics*, vol. 34, no. 6, pp. 5027-5031, Jun. 2019, doi: 10.1109/TPEL.2018.2881454.
- [17] E. Laloya, Ó. Lucía, H. Sarnago, and J. M. Burdío, "Heat management in power converters: from state of the art to future ultrahigh efficiency systems," in *IEEE Transactions on Power Electronics*, vol. 31, no. 11, pp. 7896-7908, Nov. 2016, doi: 10.1109/TPEL.2015.2513433.
- [18] Components101, "Selecting the right heat sink for your design – steps for heat sink calculation and selection," *Components101*. [Online]. Available: <https://components101.com/articles/selecting-the-right-heatsink-for-your-design-and-steps-for-heatsink-calculation-and-selection>.
- [19] A. T. de Almeida, F. J. T. E. Ferreira, and G. Baoming, "Beyond induction motors – technology trends to move up efficiency," *49th IEEE/IAS Industrial and Commercial Power Systems Technical Conference*, 2013, pp. 1-13, doi: 10.1109/ICPS.2013.6547330.
- [20] H. A. Zarchi, H. M. Hesar, and M. A. Khoshhava, "Online maximum torque per power losses strategy for indirect rotor flux-oriented control-based induction motor drives," *IET Electric Power Applications*, vol. 13, no. 2, pp. 259-265, 2019, doi: 10.1049/iet-epa.2018.5403.
- [21] D. -H. Jang and D. -Y. Yoon, "Space-vector PWM technique for two-phase inverter-fed two-phase induction motors," in *IEEE Transactions on Industry Applications*, vol. 39, no. 2, pp. 542-549, 2003, doi: 10.1109/TIA.2003.809448.
- [22] R. M. Das and E. C. Sekaran, "A cloud system model employing random space vector pulse width modulation for noise reduction in VSI fed induction motor," *Cluster Computing*, vol. 22, no. 1, pp. 347-360, 2019, doi: 10.1007/s10586-018-1956-y.
- [23] J. Rodriguez and P. Cortes, *Predictive control of power converters and electrical drives*, Hoboken, NJ, USA: Wiley-IEEE Press, 2012.
- [24] I. M. Alsofyani and N. R. N. Idris, "A review on sensor less techniques for sustainable reliability and efficient variable frequency drives of induction motors," *Renewable and sustainable energy reviews*, vol. 24, pp. 111-121, 2013, doi: 10.1016/j.rser.2013.03.051.
- [25] R. Ghosh, "Performance analysis of a silicon carbide IGBT for SVM PWM induction motor drive applications," *2017 Devices for Integrated Circuit (DevIC)*, 2017, pp. 522-526, doi: 10.1109/DEVIC.2017.8074005.
- [26] M. S. Adeel, T. Izhar, and M. A. Saqib, "An efficient implementation of the space vector modulation based three phase induction motor drive," *2009 Third International Conference on Electrical Engineering*, 2009, pp. 1-6, doi: 10.1109/ICEE.2009.5173179.
- [27] J. Ying Ying, W. Xu Dong, M. Liang Liang, Y. Shu Cai, and Z. Hai Xing, "Application and simulation of SVPWM in three phase inverter," *Proceedings of 2011 6th International Forum on Strategic Technology*, 2011, pp. 541-544, doi: 10.1109/IFOST.2011.6021082.
- [28] C. S. Edrington, O. Vodyakho, M. Steurer, S. Azongha, F. Fleming, and M. Krishnamurthy, "Power semiconductor loss evaluation in voltage source IGBT converters for three-phase induction motor drives," *2009 IEEE Vehicle Power and Propulsion Conference*, 2009, pp. 1434-1439, doi: 10.1109/VPPC.2009.5289502.

BIOGRAPHIES OF AUTHORS



Ahmed Shihab Mayyahi    was born in 1988. He has received B.Sc. in Electrical Engineering in 2011 from Electrical Engineering Department, College of Engineering, University of Diayla, Iraq. He is currently pursuing a master's study at Al-Mustansiriyah University, College of Electrical Engineering, Baghdad, Iraq. His research interests include power electronics and electrical machine. He can be contacted at email: eema2002@uomustansiriyah.edu.iq.



Riyadh Ghanem Omar    is an Assist. Prof. in the Electrical Engineering Department, Mustansiriyah University, Baghdad-Iraq, for 18 years in Power System Analysis and Power Electronics. He is a member of the electrical engineering department council. He has many publications mainly in power electronics and predictive control. He can be contacted at email: riyadh.g.omar@uomustansiriyah.edu.iq.